J Mol Hist (2007) 38:425–433
DOI 10.1007/s10735-007-9137-y

ORIGINAL PAPER

Sustained release and osteogenic potential of heparan sulfate-doped fibrin glue scaffolds within a rat cranial model

Maria Ann Woodruff · Subha Narayan Rath · Evelyn Susanto · Larisa M. Haupt · Dietmar W. Hutmacher · Victor Nurcombe · Simon M. Cool

Received: 5 June 2007 / Accepted: 20 August 2007 / Published online: 12 September 2007

Abstract This paper explores the potential therapeutic role of the naturally occurring sugar heparan sulfate (HS) for the augmentation of bone repair. Scaffolds comprising fibrin glue loaded with 5 μg of embryonically derived HS were assessed, firstly as a release-reservoir, and secondly as a scaffold to stimulate bone regeneration in a critical size rat cranial defect. We show HS-loaded scaffolds have a uniform distribution of HS, which was readily released with a typical burst phase, quickly followed by a prolonged delivery lasting several days. Importantly, the released HS contributed to improved wound healing over a 3-month period as determined by microcomputed tomography (μCT) scanning, histology, histomorphometry, and PCR for osteogenic markers. In all cases, only minimal healing was observed after 1 and 3 months in the absence of HS. In contrast, marked healing was observed by 3 months following HS treatment, with nearly full closure of the defect site. PCR analysis showed significant increases in the gene expression of the osteogenic markers Runx2, alkaline phosphatase, and osteopontin in the heparin sulfate group compared with controls. These results further emphasize the important role HS plays in augmenting wound healing, and its successful delivery in a hydrogel provides a novel alternative to autologous bone graft and growth factor-based therapies.

Keywords Glycosaminoglycans · Bone regeneration · Biomaterials · CT scanning

Introduction

The drive to develop bone regenerative therapies to circumvent delayed and non-union of bone fractures is an important therapeutic issue, especially considering the millions of fractures which occur annually, at least 10% of which are unable to heal by themselves. Several growth factors play key roles in the process of bone repair, and studies aimed at elucidating the factors affecting stem cell fate have recently demonstrated that the extracellular glycosaminoglycan sugar heparan sulfate (HS) plays a key role in the proliferation and differentiation of human bone marrow-derived mesenchymal stem cells (Cool and Nurcombe 2005). Osteogenic lineage fate decisions in general are known to be strongly influenced by several heparan-binding growth factors and it is widely accepted that fibroblast growth factors (FGFs) and their receptors (FGFRs) are essential to osteoblast differentiation and proliferation (Fakhry 2005; Ornitz et al. 2002; Zhang et al. 2002). Much evidence has accumulated to show that FGF signaling, together with a large number of other growth and adhesive factors, is in fact controlled by HS (Jackson et al. 2006b).

Maria Ann Woodruff and Subha Narayan Rath contributed equally to this work.

M. A. Woodruff · S. N. Rath · E. Susanto · D. W. Hutmacher
Division of Bioengineering, Faculty of Engineering, National University of Singapore, Singapore 119260, Singapore
e-mail: biewma@nus.edu.sg

L. M. Haupt · V. Nurcombe · S. M. Cool (✉)
Stem Cells and Tissue Repair Group, Institute of Molecular and Cell Biology, Proteos, 61 Biopolis Drive, Singapore 138673, Singapore
e-mail: scool@imcb.a-star.edu.sg

D. W. Hutmacher · V. Nurcombe · S. M. Cool
Department of Orthopaedic Surgery, Yong Loo Lin School of Medicine, National University of Singapore, Singapore 119074, Singapore

Heparan sulfate is member of the glycosaminoglycan family of macromolecules. These are linear polysaccharides consisting of a repeating glucosamine/glucuronic acid disaccharide unit backbone attached to a protein core. HS has highly but variably sulfated sequences contained within its chains, organized into clusters that facilitate protein binding. These sulfated structural domain motifs are primarily responsible for the regulatory properties of HS (Guido and Bernfield 1998). HS polysaccharides display versatilities in conformation and orientation of functional groups which enable them to employ different modes of binding with protein complexes. These selective interactions with certain proteins results in regulation of protein activities (Cool and Nurcombe 2005). HS thus acts as a co-receptor, binding to heparin-binding growth factors such as FGF and BMP2, both protecting them from proteolytic degradation and promoting binding to their high-affinity receptors (Turnbull et al. 2001). HS has a low affinity yet high capacity for its ligands, drawing them onto the cell surface with their high-affinity cognate receptors, which then transduce the appropriate signal into the cells (Lyon and Gallagher 1998). Moreover, HS binding is thought to be important in providing a matrix-bound pericellular reservoir of growth factors, promoting their long-term availability to cells (Saksela and Rifkin 1989). The interaction of BMPs with their threonine-serine kinase BMP receptors is also thought to be mediated by HS (Irie et al. 2003; Takada et al. 2003; Coombe and Kett 2005). And furthermore HS is thought to prevent diffusion of BMP2 in vivo, away from the regions where is it likely to be required (Depprich et al. 2005).

Due to its ability to bind and potentiate bioactive molecules, there is growing evidence that the ECM-derived HS may prove to be a valuable adjunct for a variety of tissue engineering and wound-healing strategies that currently use growth factor treatments (Coombe and Kett 2005). HS and its mimetics have been shown to improve bone regeneration when added exogenously in both long bone healing (Jackson et al. 2006a) and cranial defect models (Blanquaert et al. 1995; Lafont et al. 2004). HS mimetics applied to a cranial defect model have shown an increase in new bone formation and neovascularization in the wound area over the first 5 days after injury. A single dose application of HS to a rat femoral fracture at the time of injury has been demonstrated to increase callus size and bone volume after only 2 weeks (Jackson et al. 2006a). Notably, these studies used single applications of HS in short-term delivery devices with promising results on the early stages of healing but triggered little difference in the later stages. Due to the temporal pattern of growth factor expression during bone repair, we have previously examined the prolonged localized delivery of HS over several days from polycaprolactone microcapsules (Luong-Van et al. 2007).

Fibrin glue enjoys widespread clinical application as a wound sealant, a reservoir to deliver growth factors and as an aid in the placement and securement of biological implants (Vasita and Katti 2006; Pandit et al. 2000; DeBlois et al. 1994). Several studies have shown that fibrin glue promotes the regrowth of peripheral nerves to levels comparable with standard microsurgery, making it a popular candidate for experimental nerve repair (Shireman and Greisler 1998). In the cellular environment, fibrin specifically binds to a variety of proteins, including fibronectin, albumin, FGF2, VEGF, and IL-1 (Fakhry 2005). These properties make it an interesting drug and cell delivery system for various applications in tissue engineering (Vasita and Katti 2006; Pandit et al. 2000; DeBlois et al. 1994; Rai et al. 2005). Previous studies have focused on capabilities with respect to tailoring the scaffold to generate release profiles of the growth factors over time. Here, we investigated the bone regenerative capabilities of a single dose of HS encapsulated within a fibrin glue scaffold when implanted into a critical sized rat calvarial defect model. In vitro, we demonstrate the distribution and release of HS from fibrin glue scaffolds. In vivo, we utilized microcomputed tomography (μCT) scanning, histological examination, and RQ-PCR of osteogenic markers to examine the effects of HS on the process of bone regeneration.

Materials and methods

Scaffold fabrication

Fibrin glue scaffolds were prepared using a commercial kit (TISSEEL kit; Baxter AG, Volkestwil, Switzerland) as per the manufacturer's instructions. The mold for the cylindrical fibrin glue scaffold was a sterile, modified 1 ml syringe (Fig. 1a, b) that enabled easy application directly into the defect site once the scaffold had polymerized, so enhancing sterility by eliminating the need to handle any of the scaffolds (Fig. 1c). Fibrinogen (25 µl) was added to 25 µl of thrombin solution, producing a polymerized scaffold of ~5 mm diameter and a thickness of 2 mm (Fig. 1d). Two different concentrations of thrombin (thrombins 4 and 500) were investigated in vitro to optimize for the onset of in vivo experiments. The fibrin glue scaffolds created were used as a carrier-matrix for the HS delivery as well as to fill up the bone defect site. To incorporate HS into the scaffold, 5 µg (HS) was added to the thrombin component. This was thoroughly mixed and then pipetted into the sterile modified syringe body before

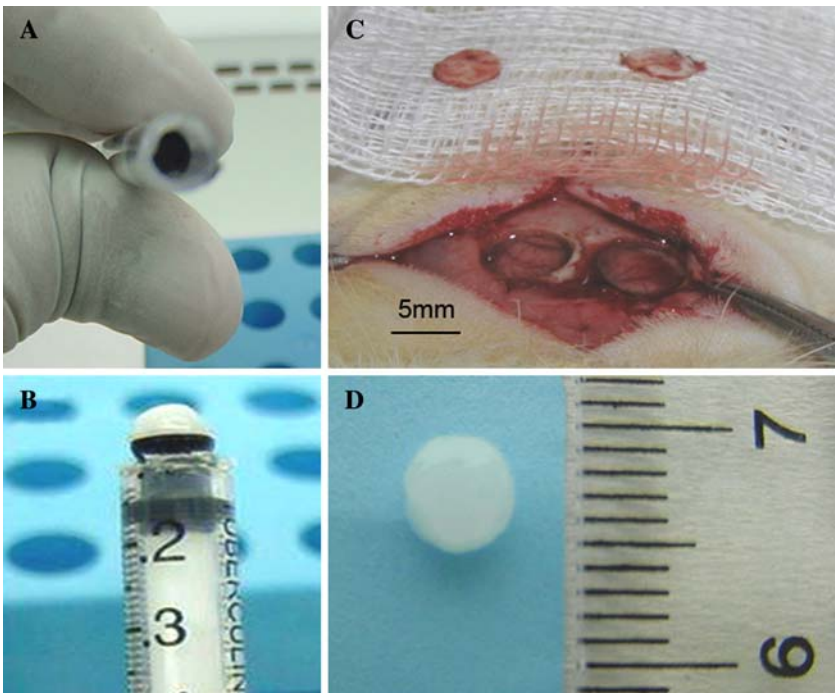

Fig. 1 Fibrin glue scaffold fabrication. Thrombin, fibrinogen, and HS were mixed and polymerized in the barrel of a 1 ml modified syringe (**a**) and ejected after production (**b**). The sterile fibrin scaffold produced had dimensions of ~5 mm in diameter and a thickness of 2 mm (**d**), which could then be easily implanted directly into the 5 mm defect sites (**c**)

adding the fibrinogen component. The ensuing polymerization of the glue and encapsulation of the HS took ~1 h. The scaffolds were then examined in vitro for (a) HS release, to observe the release kinetics of HS from the fibrin glue; (b) confocal microscopy, to observe the distribution of HS throughout the fibrin glue scaffold; and (c) in vivo implantation and μCT evaluation of bone mineralization and histological examination. For the purpose of this study, all in vitro experiments were undertaken using Heparin (Sigma, St. Louis, MO, USA) as a control substitute for HS. Heparin is structurally similar to HS, and is believed to distribute and release in the same way within a scaffold. It can be easily conjugated to the fluorescent label Alexa Fluor-488, enabling its distribution to be localized and viewed using confocal microscopy, and its release quantified using fluorescent plate reading. All in vivo work utilized HS.

Confocal microscopy

Heparin was fluorescently conjugated with Alexa Fluor-488 (A488, Molecular probes, Eugene, OR, USA) using a method adapted from Osmond et al. (2002), prior to incorporation into the scaffold. To visualize the distribution of heparin, scaffolds were viewed using confocal laser scanning microscopy (Zeiss LSM S10 meta inverted microscope). Three-dimensional depth projections were constructed from 100 horizontal slices of step size 10 μm.

Release kinetics

Fibrin glue scaffolds containing 5 μg Alexa Fluor-488-labeled heparin were placed into 1 ml of pre-warmed phosphate buffered saline (PBS) and incubated at 37°C, protected from light, for a 7-day period. At each time point, 100 μl of PBS was removed for sampling and replaced with fresh PBS. The heparin released was quantified from the fluorescence intensity of the release media at 485 nm by comparison with a standard Alexa Fluor-488-heparin curve. The cumulative release was then graphed.

Surgery

The in vivo study involved the creation of two 5 mm diameter defects in the parietal bone. About 20 female Wistar rats (300–400 gm) were used with approval from the Institutional Animal Care and Use Committee (IACUC), Singapore. They were randomly divided into three groups: (a) empty defects, (b) fibrin glue defects containing fibrin glue scaffold alone, and (c) fibrin glue defects containing fibrin glue scaffold encapsulated HS (5 μg).

Prior to surgery, the rats were given intra-peritoneal anesthesia of 75 mg/kg Ketamine and 1 mg/kg Medetomidine, the heads were shaved and saline-soaked gauze applied across the eyes. Under aseptic technique, the skin over the calvaria was disinfected with Betadine™, the skin

over the parietal bone dissected in the sagittal plane and the periosteum removed from the both sides of the parietal bone. As previously described, a 5 mm diameter trephine was used to create two circular through-and-through, critical-sized bony defects which were irrigated with saline to remove blood clots; hemostasis was achieved with gentle pressure. The fibrin glue scaffolds ±HS were applied directly into the defect sites utilizing the novel syringe system. The skin was closed with 5–0 absorbable coated vicryl sutures (polyglactin 910, Johnson and Johnson, New Brunswick, NJ, USA). The animals were then given reverse anesthetics (5 mg/ml of anti-sedan), antibiotics, and temegesic pain killers. They were placed individually in cages with food and water, and observed postoperatively for adverse effects.

Microcomputed tomography (μCT) scanning

At 1 and 3 months after surgery, the rats were anesthetized intra-peritoneally as previously described before undergoing μCT scanning to obtain a quantitative measure of the levels of regenerated bone (SKYSCAN-1076 in vivo microcomputerized tomography scanner, Belgium). As previously described, imaging was performed with 68 mm scan width, an Al 1 mm filter, 35 μm pixel size, using an average of four sets of scan data per sample (Shao et al. 2006). All samples were scanned through a 180° rotation angle with a rotation step of 0.8° at 35 μm resolution. The data were volumetrically reconstructed using cone beam CT reconstruction software from SKYSCAN at 1,968 × 1,968 pixels. Files were then reconstructed for analysis by Mimics v 8.11 software (Materialize, Flanders, Belgium) using in-built functions. From the three-dimensional image, a cylindrical region of interest (ROI) of defect size of 5 mm diameter was selected for analysis. This ROI corresponds to the original defect location. The degree of bone regeneration occurring within the defect was presented as a volume in mm^3 of reconstructed data obtained in microCT analysis. The threshold was adjusted empirically to visualize the defect site and the mineralization and was then kept constant for every sample (-284 to 1,420 HUs for all reconstructions). Defect reconstruction was attained by subtracting the scanned mineralization data.

Histology and histomorphometry

Animals were sacrificed at 3 months in a CO_2 chamber. After euthanasia, tissue was dissected from the calvarial bone and the defect site sectioned for histology. For processing, tissue was fixed in 10% neutral buffered formalin for 2 days and de-calcified in 12.5% EDTA (Sigma Aldrich) pH 7.0 for 3 weeks. The samples were then serially dehydrated in ethanol in a tissue processor (Shandon Citadel 1000, Thermo Scientific, Franklin, MA, USA), and paraffin embedded (Leica EG 1160). Sections (5 μm) were taken using a microtome (Leica RM 2135). The slides were deparaffinized with xylene and rehydrated with serial concentrations of ethanol, before being stained with haematoxylin and eosin (Sigma Aldrich) and mounted with DPX mountant (Fluka Biochemica, Milwaukee, WI, USA). Immunohistological staining was also used employing mouse monoclonal antibodies against type I collagen (Sigma Aldrich) at 1:500 dilution, osteopontin (Santa Cruz, Santa Cruz, CA, USA) 1:50 dilution, and osteocalcin (Abcam, Cambridge, UK) at 1:150 dilution. Secondary antibodies were rat absorbed anti-mouse IgG (Vector Labs, Burlingame, CA, USA). The antigens were localized using an immunoperoxidase procedure according to the manufacturer's guidelines (VECTASTAIN® ABC kit, Vector Labs). The isotype mouse IgG1 antibody was used as a negative control (Caltag Laboratories, Burlingame, CA, USA).

Histomorphometry was performed using Bioquant Osteo II software to quantify the percentage staining for collagen I, osteocalcin, and osteopontin within the defect site. Briefly, a ROI was manually drawn around the defect site. The entire defect site was first quantified (total area), and then the percentage of positive stain for each of the aforementioned proteins was quantified and expressed as a percentage of the entire defect site. This positive stain was obtained by manually thresholding the images and directing the software to pick up only the positive stains attributable to the protein of interest (attained through comparisons with negative controls). The thresholds were saved and applied to every slide within the data set, for each stain.

RNA isolation and RQ-PCR

Following sacrifice of the animals, the defect sites were surgically collected and immediately frozen using liquid nitrogen. The extracted tissue was then ground to powder form with a mortar and pestle. Total RNA was extracted using Trizol reagent (Invitrogen Corp., Carlsbad, CA, USA) and subsequent clean up using an RNeasy Mini Kit (QIAGEN, Singapore, Singapore) according to the manufacturer's instructions. The quality of the isolated RNA was assessed by gel electrophoresis and quantitated on a Genequant RNA/DNA Spectrophotometer (Amersham Biosciences, Piscataway, NJ, USA) and stored at –80°C until further use. For conversion to cDNA, 500 ng of total RNA was reverse-transcribed using random hexamers

catalyzed by Superscript III RT (Invitrogen Corp.). Following spectrophometric quantitation of the cDNA, expression levels of the target genes were determined using RQ-PCR. Briefly, 120 ng of cDNA was amplified using the ABI Prism FAST 7500® sequence detection system (Perkin-Elmer Life Sciences, Wellesley, MA, USA) using the default cycle: 95°C × 20 s followed by 40 cycles of 95°C × 3 s, 60°C × 30 s. Runx2, osteopontin and 18S primers and probes were designed using Primer Express software (v 2.1, PE Applied Biosystems, Foster City, CA, USA), and have been described elsewhere (Ng et al. 2007). Alkaline phosphatase primer and probes were purchased as an Assay-on-demand (PE Applied Biosystems). The Runx2 and osteopontin LNA probes were re-designed to incorporate LNA bases and labeled with BHQ-1 (Proligo, Singapore, Singapore). The ribosomal subunit gene 18S (VIC/TAMRA, Foster City, CA, USA) was used as the endogenous control. Data was analyzed using the ABI Sequence Detector software. Amplifications were performed three times in triplicate. Target gene expression values were calculated relative to the endogenous control 18S expression levels using the ($2^{(-DDCt)}$) calculation.

Statistical analysis

A two-way ANOVA with differences considered significant at the 95% confidence interval, was used to determine significant differences between mineralization within the HS and non-HS treated scaffolds followed by the Bonferroni post-test. Standard error bars were included in all graphs and represent the 95% confidence interval.

Results

In vitro analysis of HS-loaded fibrin glue scaffolds

To examine the distribution of heparin through the fibrin scaffold and to assess its time-release, a combination of confocal microscopy and fluorescent spectroscopy was performed. Confocal microscopy demonstrated a uniform distribution of heparin (HS substitute) throughout the fibrin scaffold. Sequential scans of 10 μm slices were taken and showed no significant change in heparin distribution between each slice throughout the whole body of the scaffold (data not shown). However, following several trials, the polymerization rate of thrombin 500 was determined to be too rapid, prone to air bubbles and uneven encapsulation of the heparin component.

When we compared the release kinetics of heparin from the scaffold, using both thrombins 4 and 500 components, similarities were observed. The release from both scaffolds followed the same pattern; a fast initial burst with over 50% release within the first 4 h, followed by a sustained release over the course of 4 days, at which time 100% of the heparin had been released (Fig. 2). As a result only the thrombin 4 dosed scaffolds were used for the in vitro analyses.

In vivo analysis of HS-loaded fibrin glue scaffolds

The effect of HS on augmenting in vivo bone healing was first assessed by μCT and histomorphometry. MicroCT scanning detected an increase in mineralization for those defect sites treated with HS at both 1 and 3 months. Representative reconstructions of the defect sites at 1 and 3 months for all treatments are presented in Fig. 3. All treatments demonstrated significant increases from months

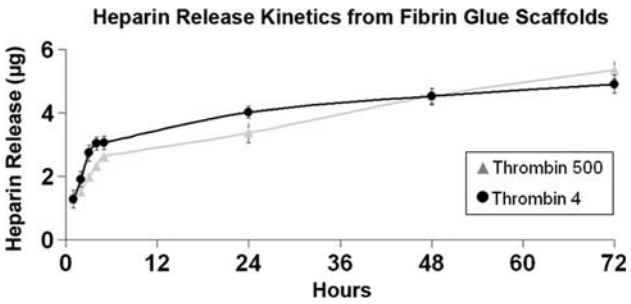

Fig. 2 In vitro analysis of release kinetics of Alexa-468-heparin from fibrin scaffolds revealed a sharp initial burst of over 50% total heparin released in the first 4 h followed by a sustained release of up to 100% over 4 days. *Filled triangle* thrombin 500, *filled circle* thrombin 4

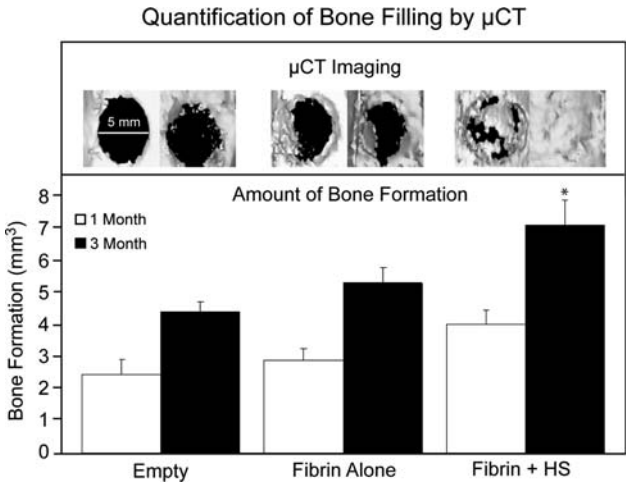

Fig. 3 Quantified μCT analysis of defect sites at 1 and 3 months for empty defect sites, fibrin glue alone and HS treated sites. Representative μCT images were analyzed using MIMICs evaluation of the total volume of mineralized bone, in mm^3, detected within the defect sites. *Asterisk* denotes a significant difference between HS treated sites and all other defect sites at 3 months

1 to 3 within their respective groups. At 3 months the HS-treated sites had full closure of the defect with mineralized bone. When quantiated using the MIMICs software, significantly higher mineralized bone was present in the HS treated sites at 3 months when compared with empty defect sites and fibrin glue alone defect sites ($p < 0.05$). No significant differences were observed between the treatment groups after 1 month.

We then examined the isolated and sectioned samples histologically using hematoxylin and eosin (H&E) staining and immunohistochemistry. The fibrin glue alone defect sites appear to have residual bone chips present from surgery, possibly owing to incomplete drilling through the parietal bone, and appear to be composed of newly formed bone with more intense and uniform staining, containing sparse non-contiguous islands within the defect area (Fig. 4b). The empty defects appear to have only sparse fibrous connective tissue bridging between the bony fronts (Fig. 4a). In the HS treated samples, newly formed, contiguous bone can be observed with and surrounding all edges of the defect site (Fig. 4c). The osteogenic markers collagen type I, osteocalcin, and osteopontin all gave demonstrably higher staining within the HS treated groups when compared with empty defects. Collagen I was lowly detectable and disordered in both the empty and fibrin glue defect sites (Fig. 4d, e). In contrast, in the HS-treated samples, collagen I had a more organized and fibrillar appearance along the direction of the fibrous tissue, contiguous with the structured bone edges of the defect site (Fig. 4f). Osteocalcin staining was very low in both the empty and fibrin defect sites, with signal detected predominantly in the bone edges of the defect site (Fig. 4g, h). In the HS-treated defect sites, osteocalcin staining was uniform throughout both the bone edges and the repaired defect site (Fig. 4j). Osteopontin was very low in the empty defect samples (Fig. 4j) but was present throughout the fibrin-treated defects (Fig. 4k). The distribution of osteopontin throughout the HS-treated defects appeared to be mostly localized to the bone edges (Fig. 4l). When we quantified the staining within the defect sites using Bioquant analyses, these observations were reinforced with HS-treated defects determined to have significantly higher levels of collagen type I, osteocalcin, and osteopontin at 3 months (Fig. 5).

RQ-PCR analysis of treatment sites

To further assess bone formation, we examined the osteogenic markers Runx2, alkaline phosphatase, and osteopontin using RQ-PCR in the fibrin glue and HS treated samples. As expected, the fibrin glue alone samples

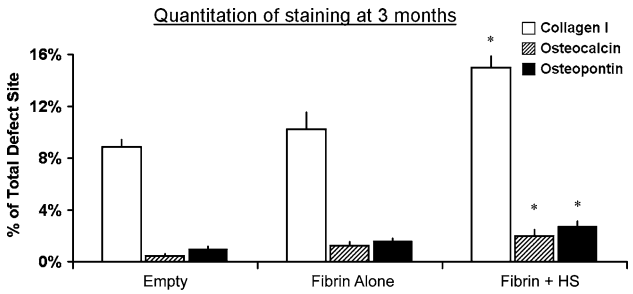

Fig. 5 Quantitation of staining as a percentage of total tissue formation after 3 months determined using Bioquant image analysis software. *Asterisk* denotes a significant difference between HS treated sites and all other sites

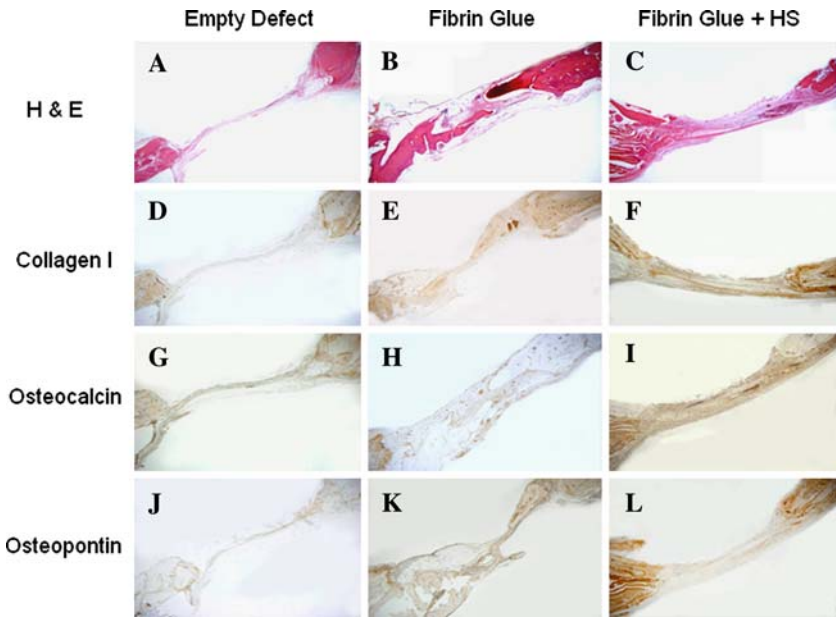

Fig. 4 Representative photographs of tissue section analysis of haemotoxylin and eosin (**a–c**), and immunohistochemistical staining for type I collagen (**d–f**), osteocalcin (**g–i**), and osteopontin (**j–l**) within each defect site after 3 months

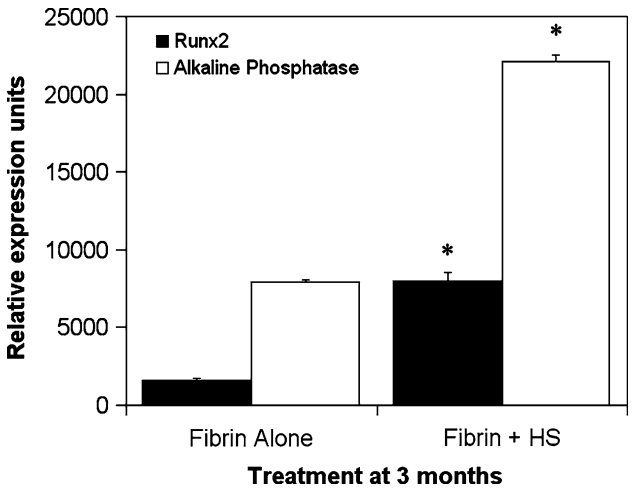

Fig. 6 RQ-PCR analysis of osteogenic markers showing Runx2 and alkaline phosphatase expression comparing tissue from defect sites with fibrin glue alone and HS fibrin glue scaffolds at 3 months

demonstrated expression of all three osteogenic markers examined, confirming the presence of osteogenic-committed cells within the isolated defect sites. Significant up-regulation of all markers was demonstrated in the HS-treated samples. Notably, Runx2 was up-regulated sixfold, alkaline phosphatase threefold, and osteopontin twofold (data not shown). The comparison of the Runx2 and alkaline phosphatase data are presented in Fig. 6.

Discussion

Bone is a dynamic and multifunctional organ capable of remodeling and self-regeneration. However, in extreme cases of non-union or delayed fracture union, therapeutic intervention is often required. In conventional procedures, the transplantation of bone requires invasive procedures including skin and mucosal incisions and resection of the periosteum. The ability to implant a bioactive scaffold with osteoinductive properties within a critical sized defect is an attractive one, especially if the therapy negates the requirement to include live cells in the scaffold.

It has been shown that the local or systemic application of a number of growth factors such as FGF2 and BMP2 (Fakhry 2005; Blanquaert et al. 1995) can aid bone repair. Disadvantages of such applications include their rapid clearance rates and susceptibility to proteolytic degradation (Babensee et al. 2000). Additionally there is concern over their long-term safety and associated costs, particularly as large quantities are required. HS binds to a variety of soluble proteins involved in the control of cell phenotype, including heparin-binding growth factors. The HS mode of action is to concentrate growth factors close to cells, protect them from extracellular proteases, shepherd them to the cell surface and facilitate binding to their specific receptors (Zhang et al. 2002). The complexes formed can be readily dissociated and mobilized in the event of tissue damage, resulting in prolonged bioactivity at the site of damage (Coombe and Kett 2005). HS has been implicated in facilitating and stabilizing the interaction of FGFs with their receptors. The more complicated interaction with BMPs have been demonstrated to include a stabilizing and storage role in the extracellular space (Ruppert et al. 1996), maintaining the growth factor spatially away from it's receptor, thus limiting signaling potential (Takada et al. 2003) and preventing diffusion from a site of injury (Depprich et al. 2005), however these interactions act in unison to modulate the activity and it has not yet been shown that HS interacts directly with the BMP2/receptor complex. Nontheless, a synergistic interaction seems apparent between HS and BMP2, although the exact mechanism driving this is still unknown. We and others, have previously demonstrated increased bone regeneration through addition of HS and HS-like molecules. Heparan-like mimetics (carboxymethy-lbezylamide-sulfonated dextrans) have been reported to induce the repair of rat skull defects (Lafont et al. 2004), and single doses of HS have been shown to augment fracture repair in a rat model (Jackson et al. 2006a).

Fibrin glue is a physiologically relevant matrix whose principle component, fibrin, has fundamental roles in the process of blood clotting and wound healing. It is also a potentially suitable biological vehicle for cell transplantation, as it has proven biocompatibility, biodegradability and binding capacity to cells (Mundlos et al. 1997). Fibrin stabilizing factor XIII, contained in fibrin glue, favors migration of undifferentiated mesenchymal cells on the highly cross-linked structure of the glue and it enhances proliferation of these cells (Otto et al. 1997; Choi et al. 2005). The fibrin glue scaffolds in this study were comprised of a low concentration of thrombin (thrombin 4), as the suitability and incorporation of the HS into the polymerizing glue proved difficult using higher concentrations (thrombin 500). Increasing the thrombin concentration has previously been demonstrated to affect fiber thickness, porosity, and homogeneity of the fibrin (Pratap et al. 2003). Given the promising therapeutic potential of HS, this study sought to investigate the effects of HS on bone regeneration within a critical sized rat cranial defect using fibrin glue as a release reservoir.

Initial in vitro studies demonstrated heparin (the control for HS) was released rapidly in the first 4 h from the fibrin glue scaffolds, with over 50% of the total heparin released in the first 4 h, followed by a sustained release (up to 100% over 4 days). When applied in vivo, this sharp burst may provide a large, initial stimulus for growth factor recruitment and concentration and thus an accelerated onset of

bone regeneration. Although the HS is not physically attached to the scaffold, and probably diffuses away from the wound site fairly rapidly, it appears that the initial high presence (~5 μg) of HS within the site of injury is sufficient enough to stimulate an enhanced regenerative response. Indeed, the local gradient of HS within the vicinity of the wound site may provide an environment which produces a corresponding gradient of growth factors, a known stimulator for migrating cells. Such gradients may affect subsequent wound healing by guaranteeing a store of pre-activated growth factors immediately adjacent to the wound site, which in turn would act to stimulate the recruitment of more stem cells into the wound site.

We next examined how to determine the best doses and release profiles required for optimal bone regeneration over a longer period in vivo. We utilized μCT scanning to determine bone mineralization within the defect sites and reinforced this with histological and histomorphometrical examination of the defect sites and gene expression analyses of isolated tissue.

MicroCT analysis showed significant bone regeneration within defects treated with HS compared to empty defects and fibrin glue alone, with full closure of sites observed after 3 months. Histological analysis showed clear differences in tissue formation among the different treatment conditions. Sparse fibrous connective tissue was found to traverse the empty defects, compounded by the lowest levels of staining for collagen I, osteocalcin, and osteopontin. In contrast, in the HS treated samples, newly formed bone was clearly observed surrounding all edges of the defect site, with contiguous bone within the defect site demonstrating intense and uniform staining for the osteogenic markers. Quantitative analysis reinforced the observed immunohistochemical data with significantly higher levels of collagen I, osteocalcin, and osteopontin within the HS-treated defect sites. Additionally, using RQ-PCR, gene expression of key osteogenic markers was also demonstrated, with increased Runx2, alkaline phosphatase, and osteopontin in the HS treated groups. It is of note that due to the amount of tissue available, the yield and quality of extracted RNA from the empty defect sites was significantly lower than the other treatment conditions. Runx2 is regarded as the key regulator of osteogenesis and has been shown to be essential for skeletal patterning during embryogenesis and the progression of osteoblast differentiation (Keller et al. 1985; Kasai et al. 1983; Marktl and Rudas 1974; Le Nihouannen et al. 2006; Ducy et al. 1999). Calvarial cells harvested from Runx2-deficient mice have increased rates of cell proliferation, DNA synthesis, and G1/S phase markers; the reintroduction of Runx2 restores normal cell cycling, emphasizing the importance of Runx2 for cell cycle regulation (Komori et al. 1997). Reports have suggested the addition of HS can increase the expression of Runx2, alkaline phosphatase, and osteopontin in pre-osteoblast cells, suggesting the potential for exogenous HS to shift cells from proliferative to differentiative phenotypes (Jackson et al. 2006b). These results are consistent with this hypothesis.

The current study evaluated a previously verified dose of HS encapsulated within a fibrin glue delivery system, for its ability to influence sustained bone repair within critical sized rat cranial defects. Our results suggest that by enhancing growth factor activity within the defect site, HS mediates increased bone repair reflected by increased mineralized bone and osteogenic marker expression. These data suggests the HS may have a significant therapeutic role in bone regeneration.

Acknowledgments The authors would like to thank Amber Annettte Sawyer for training with Bioquant image analysis software.

References

Babensee JE, McIntyre LV, Mikos AG (2000) Growth factor delivery for tissue engineering. Pharm Res 17:497–504

Blanquaert F, Saffar JL, Colombier ML, Carpentier G, Barritault D, Caruelle JP (1995) Heparan-like molecules induce the repair of skull defects. Bone 17:499–506

Choi KY, Kim HJ, Lee MH, Kwon TG, Nah HD, Furuichi T, Komori T, Nam SH, Kim YJ, Kim HJ, Ryoo HM (2005) Runx2 regulates FGF2-induced Bmp2 expression during cranial bone development. Dev Dyn 233(1):115–121

Cool SM, Nurcombe V (2005) The osteoblast-heparan sulfate axis: control of the bone cell lineage. Int J BiochemCell Biol 37(9):1739–1745

Coombe DR, Kett WC (2005) Heparan sulfate-protein interactions: therapeutic potential through structure-function insights. Cell Mol Life Sci 62:410–424

DeBlois C, Cote MF, Doillon CJ (1994) Heparin-fibroblast growth factor fibrin complex: in vitro and in vivo applications to collagen based materials. Biomaterials 15(9):665–672

Depprich R, Handschel J, Sebald W, Kubler NR, Wurzler KK (2005) Comparison of the osteogenic activity of bone morphogenetic protein (BMP) mutants. Mund Kiefer Gesichtschir 9:363–368

Ducy P, Starbuck M, Priemel M, Shen J, Pinero G, Geoffroy V, Amling M, Karsenty G (1999) A Cbfa1-dependent genetic pathway controls bone formation beyond embryonic development. Genes Dev 13(8):1025–1036

Fakhry A (2005) Effects of FGF-2/-9 in calvarial bone cell cultures: differentiation stage-dependent mitogenic effect, inverse regulation of BMP-2 and noggin, and enhancement of osteogenic potential. Bone 36:254–266

Guido D, Bernfield M (1998) The emerging roles of cell surface heparan sulfate proteoglycans. Matrix Biol 17(7):461–463

Irie A, Habuchi H, Kimata K, Sanai Y (2003) Heparan sulfate is required for bone morphogenetic protein-7 signaling. Biochem Biophys Res Commun 308:858–865

Jackson RA, McDonald MM, Nurcombe V, Little DG, Cool SM (2006a) The use of heparan sulfate to augment fracture repair in a rat fracture model. J Orthop Res 24:636–644

Jackson RA, Nurcombe V, Cool SM (2006b) Coordinated fibroblast growth factor and heparan sulfate regulation of Osteogenesis. Gene 379:79–91

Kasai S, Kunimoto T, Nitta K (1983) Cross linking of fibrin by activated factor XIII stimulates attachment, morphological changes and proliferation of fibroblasts. Biomed Res 4:155–160

Keller J, Anderasses TT, Joyce F (1985) Fixation of osteochondral fractures: fibrin sealant tested in dogs. Acta Orthop Scand 56:323–326

Komori T, Yagi H, Nomura S, Yamaguchi A, Sasaki K, Deguchi K, Shimizu Y, Bronson RT, Gao YH, Inada M, Sato M, Okamoto R, Kitamura Y, Yoshiki S, Kishimoto T (1997) Targeted disruption of Cbfa1 results in a complete lack of bone formation owing to maturational arrest of osteoblasts. Cell 89(5):755–764

Lafont J, Blanquaert F, Colombier ML, Barritault D, Carueelle JP, Saffar JL (2004) Kinetic study of early regenerative effects of RGTA11, a heparan sulfate mimetic, in rat craniotomy defects. Calcif Tissue Int 75:517–525

Le Nihouannen D, Le Guehennen L, Rouillon T, Pilet P, Bilban M, Layrolle P, Daculsi G (2006) Micro-architecture of calcium phosphate granules and fibrin glue composites for bone tissue engineering. Biomaterials 27:2716–2722

Luong-Van E, Grøndahl L, Nurcombe V, Cool SM (2007) In vitro biocompatibility and bioactivity of microencapsulated heparan sulfate. Biomaterials 28:2127–2136

Lyon M, Gallagher JT (1998) Bio-specific sequences and domains in heparan sulfate and the regulation of cell growth and adhesion. Matrix Biol 17(7):485–493

Marktl W, Rudas B (1974) The effect of factor XIII on wound granulation in the rat. Thromb Diath Haemorrh 32:578–581

Mundlos S, Otto F, Mundlos C, Mulliken JB, Aylsworth AS, Albright S, Lindhout D, Cole WG, Henn W, Knoll JH, Owen MJ, Mertelsmann R, Zabel BU, Olsen BR (1997) Mutations involving the transcription factor CBFA1 cause cleidocranial dysplasia. Cell 89(5):773–779

Ng KW, Spiecher T, Dombrowski C, Helledie T, Haupt LM, Nurcombe V, Cool SM (2007) Osteogenic differentiation of murine embryonic stem cells is mediated by fibroblast growth factor receptors. Stem Cells Dev 16:305–318

Ornitz DM, Marie PJ (2002) FGF signaling pathways in endochondral and intra-membranous bone development and human genetic disease. Genes Dev 16:1446–1465

Osmond RI, Kett WC, Skett SE, Coombe DR (2002) Protein-heparin interactions measured by BIAcore 2000 are affected by the method of heparin immobilization. Anal Biochem 310:199–207

Otto F, Thornell AP, Crompton T, Denzel A, Gilmour KC, Rosewell IR, Stamp GW, Beddington RS, Mundlos S, Olsen BR, Selby PB, Owen MJ (1997) Cbfa1, a candidate gene for cleidocranial dysplasia syndrome, is essential for osteoblast differentiation and bone development. Cell 89(5):765–771

Pandit AS, Wilson DJ, Feldman DS (2000) Fibrin scaffold as an effective vehicle for the delivery of acidic growth factor (FGF-1). J Biomater Appl 14(3):229–242

Pratap J, Galindo M, Zaidi SK, Vradii D, Bhat BM, Robinson JA, Choi JY, Komori T, Stein JL, Lian JB, Stein GS, van Wijnen AJ (2003) Cell growth regulatory cell regulatory role of Runx2 during proliferative expansion of preosteoblasts. Cancer Res 63(17):5357–5362

Rai B, Teoh SH, Hutmacher DW, Cao T, Ho KH (2005) Novel PCL-based honeycomb scaffolds as drug delivery systems for rhBMP-2. Biomaterials 26:3739–3748

Ruppert R, Hoffmann E, Sebald W (1996). Human bone morphogenetic protein 2 contains a heparin-binding site which modifies its biological activity. Eur J Biochem 237:295–302

Saksela O, Rifkin D (1989). Release of basic fibroblast growth factor-heparan sulfate complexes from endothelial cells by plasminogen activator-mediated proteolytic activity. Fibrinolysis 3:36

Shao XX, Hutmacher DW, Ho ST, Goh JC, Lee EH (2006) Evaluation of a hybrid scaffold/cell construct in repair of high-load-bearing osteochondral defects in rabbits. Biomaterials 27(7):1071–1080

Shireman PK, Greisler HP (1998) Fibrin Sealant in vascular surgery: a review. J Long Term Eff Med Implants 8:117–132

Takada T, Katagiri T, Ifuku M, Morimura N, Kobayashi M, Hasegawa K, Ogamo A, Kamijo R (2003) Sulfated polysaccharides enhance the biological activities of bone morphogenetic proteins. J Biol Chem 278:43229–43235

Turnbull J, Powell A, Guimond S (2001). Heparan sulfate: decoding a dynamic multifunctional cell regulator. Trends Cell Biol 11(2):75–82

Vasita R, Katti DS (2006) Growth factor delivery systems for tissue engineering: a materials perspective. Expert Rev Med Devices 3(1):29–47

Zhang X, Sobue T, Hurley MM (2002) FGF-2 increases colony formation, PTH receptor, and IGF-1 mRNA in mouse marrow stromal cells. Biochem Biophys Res Commun 290:526–531